Published in final edited form as:
J Comp Neurol. 2014 December 1; 522(17): 3885–3899. doi:10.1002/cne.23647.

Brain-derived neurotrophic factor but not vesicular zinc promotes TrkB activation within mossy fibers of mouse hippocampus *in vivo*

Jeffrey Helgager[1], **Yang Zhong Huang**[1], and **James O. McNamara**[1,2,3]

[1]Department of Neurobiology, Duke University Medical Center, Durham, NC, 27710, USA

[2]Department of Medicine (Neurology), Duke University Medical Center, Durham, NC, 27710, USA

[3]Department of Pharmacology and Molecular Cancer Biology, Duke University Medical Center, Durham, NC, 27710, USA

Abstract

The neurotrophin receptor, TrkB receptor tyrosine kinase, is critical to central nervous system (CNS) function in health and disease. Elucidating the ligands mediating TrkB activation *in vivo* will provide insights into its diverse roles in the CNS. The canonical ligand for TrkB is brain-derived neurotrophic factor (BDNF). A diversity of stimuli also can activate TrkB in the absence of BDNF, a mechanism termed transactivation. Zinc, a divalent cation packaged in synaptic vesicles along with glutamate in axons of mammalian cortical neurons, can transactivate TrkB in neurons and heterologous cells *in vitro*. Yet the contributions of BDNF and zinc to TrkB activation *in vivo* are unknown. To address these questions, we conducted immunohistochemical (IHC) studies of the hippocampal mossy fiber axons and boutons using an antibody selective for pY816 of TrkB, a surrogate measure of TrkB activation. We found that conditional deletion of BDNF resulted in a reduction of pY816 in axons and synaptic boutons of hippocampal mossy fibers, thereby implicating BDNF in activation of TrkB *in vivo*. Unexpectedly, pY816 immunoreactivity was increased in axons but not synaptic boutons of mossy fibers in ZnT3 knockout mice that lack vesicular zinc. Marked increases of BDNF content were evident within the hippocampus of ZnT3 knockout mice and genetic elimination of BDNF reduced pY816 immunoreactivity in these mice, implicating BDNF in enhanced TrkB activation mediated by vesicular zinc depletion. These findings support the conclusion that BDNF but not vesicular zinc activates TrkB in hippocampal mossy fiber axons under physiological conditions.

Corresponding author: James O. McNamara, M.D., Phone: 919-684-4241, jmc@neuro.duke.edu.

CONFLICT OF INTEREST STATEMENT

The authors state no conflict of interest.

ROLE OF AUTHORS

All authors had full access to all the data in the study and take responsibility for the integrity of the data and the accuracy of the data analysis. **Study concept and design:** Jeffrey Helgager, Yang Zhong Huang, James O. McNamara. **Acquisition of data:** Jeffrey Helgager. **Analysis and interpretation of data:** Jeffrey Helgager and James O. McNamara. **Drafting of the manuscript:** Jeffrey Helgager, Yang Zhong Huang, and James O. McNamara. **Critical revision of the manuscript for important** intellectual content: Jeffrey Helgager, Yang Zhong Huang, and James O. McNamara. **Statistical analysis:** Jeffrey Helgager. **Administrative, technical, and material support:** Jeffrey Helgager, Yang Zhong Huang, and James O. McNamara.

Note that red/green figures are provided as magenta/green in supplementary materials.

Keywords

neurotrophin; TrkB; hippocampus; mossy fiber; zinc; immunohistochemistry

INTRODUCTION

TrkB is a tyrosine kinase receptor in the tropomyosin-related kinase (Trk) family of neurotrophin receptors. Its diverse contributions to CNS function in health and disease underscores the importance of identifying the ligands which mediate its activation (Chao et al., 2006; Huang and Reichardt, 2001; McAllister et al., 1999; McNamara et al., 2006; Poo, 2001). The canonical ligand that activates TrkB is brainderived neurotrophic factor (BDNF) (Barbacid, 1995; Cunningham and Greene, 1998). BDNF is a 14 kDa protein packed in large dense-core vesicles of axons and presumably released in a neuronal activity-dependent manner (McAllister et al., 1999; Huang and Reichardt, 2001). The binding of BDNF to the ectodomain of TrkB triggers receptor dimerization and subsequent phosphorylation of tyrosines within its intracellular domain, leading to activation of TrkB signaling (McAllister et al., 1999; Huang and Reichardt, 2001). Thus measures of phosphorylation of distinct tyrosine residues (pTrkB) provide a surrogate measure of TrkB activation (Segal et al., 1996). Despite the well-established role of BDNF as the canonical TrkB ligand, however, few studies have directly addressed the contribution of endogenous BDNF to TrkB activation *in vivo*. One such study employed mice with a conditional deletion of BDNF from cells of stratum lucidum of hippocampus, where the mossy fiber axons of dentate granule cells synapse on CA3 pyramidal neurons (He et al., 2004).

Transactivation is a process by which a ligand activates a receptor without interacting directly with it (Carpenter, 1999). TrkB can undergo transactivation in response to a diversity of stimuli, including G-protein coupled receptor ligands (Jeanneteau and Chao, 2006) and epidermal growth factor (Puehringer et al., 2013). We reported that the divalent cation, zinc, can transactivate TrkB in cultured cortical neurons and heterologous cells through a BDNF-independent mechanism (Huang et al., 2008). Zinc is present in glutamate-containing synaptic vesicles of axon terminals throughout hippocampus and neocortex (Frederickson and Danscher, 1990; Choi and Koh, 1998; Frederickson et al., 2005). It is incorporated into these vesicles by zinc transporter protein-3 (ZnT3), and co-released with glutamate in an activity dependent fashion (Choi and Koh, 1998; Frederickson and Danscher, 1990; Frederickson et al., 2005). Vesicular zinc is highly concentrated in boutons of the mossy fiber axons of the dentate granule cells in stratum lucidum, but whether vesicular zinc in these boutons contributes to TrkB activation *in vivo* remains to be tested.

The objective of this study was to examine the contributions of both BDNF and vesicular zinc to TrkB activation within stratum lucidum of mouse hippocampus under physiological conditions. To this end, two strains of genetically modified mice were utilized: (1) a conditional knockout of BDNF which eliminates it from hippocampal dentate granule and CA3 pyramidal cells (He et al., 2004), and (2) a knockout of ZnT3 (Cole et al., 1999), which eliminates vesicular zinc from CNS neurons. We conducted immunohistochemical studies of TrkB activation in hippocampal mossy fiber axons and boutons using an antibody detecting

phosphorylated tyrosine residue 816 (pY816) (Helgager et al., 2013) in wild type and mutant mice.

MATERIALS AND METHODS

Generation of BDNF Mutant, ZnT3 Mutant, and ZnT3/BDNF Double Mutant Mice

Before use in experiments, all mouse lines were backcrossed for at least seven generations into a C57/BL6 background, the founders of which were originally obtained from Charles River (Wilmington, MA). *BDNF* mutant mice were generated as described in (Monteggia et al., 2004; Zhu et al., 2001), a gift from the lab of Luis Parada (University of Texas Southwestern Dallas, TX, RRID:MGI_MGI:3051987 and MGI_MGI:2176767). Cre/loxP technology (Gu et al., 1994) was utilized in these animals, and to this end exon five of the *BDNF* gene was flanked by two *loxP* sites ("floxed") so that it would be deleted in the presence of Cre recombinase. These animals were bred to transgenic mice expressing Cre recombinase under the control of a *synapsin-1* promoter (Syn-Cre). Mice homozygous for *BDNF* floxed alleles which also contain Syn-Cre (Syn-Cre^{+}/BDNF$^{flox/flox}$) will have BDNF protein eliminated from a subset of CNS neurons. In the hippocampus this results in elimination of *BDNF* gene expression in virtually all dentate granule cells and CA3 pyramidal neurons and in a subset of CA1 pyramidal cells (see Figure 1 of He et al., 2004). These conditional knockout animals will henceforth be referred to as BDNF$^{-/-}$ mice. BDNF$^{-/-}$ animals were generated by crossing Syn-Cre^{+}/BDNF$^{flox/wt}$ with Syn-Cre^{-}/BDNF$^{flox/flox}$ mice, yielding litters in which approximately 50% of animals do not contain Syn-Cre (Syn-Cre^{-} /BDNF$^{flox/wt}$ or Syn-Cre^{-}/BDNF$^{flox/flox}$) and therefore express BDNF at wild type levels, henceforth referred to as BDNF$^{+/+}$ mice, 25% are BDNF$^{+/-}$, and 25% BDNF$^{-/-}$ (He et al., 2004).

ZnT3 mutant mice, generated as described in Cole et al. (1999) were obtained from the Jackson Laboratory (Bar Harbor, ME, RRID:MGI_MGI:3029270). These animals contain a targeted deletion in which exons 1–4 of the *ZnT3* gene have been replaced with a cassette containing *nlacZ* and *neo^{r}*. Mice homozygous for this mutant allele (ZnT3$^{-/-}$) express no ZnT3 protein. By breeding those heterozygous for the mutant allele (ZnT3$^{+/-}$) together, litters were generated of approximately 25% wild type (ZnT3$^{+/+}$), 50% heterozygotes (ZnT3$^{+/-}$), and 25% nulls (ZnT3$^{-/-}$). *ZnT3/BDNF* double mutant animals (ZnT3$^{-/-}$/Syn-Cre^{+}/BDNF$^{flox/flox}$) were generated using a similar breeding strategy as done to establish BDNF$^{-/-}$ mice. Specifically, ZnT3$^{-/-}$/Syn-Cre^{-}/BDNF$^{flox/flox}$ animals were mated with ZnT3$^{-/-}$/SynCre^{+}/BDNF$^{flox/wt}$ mice. As for *BDNF* mutant animals, this strategy resulted in litters in which approximately 50% of mice do not express Syn-Cre and therefore express BDNF protein at wild type levels, though are knockouts of *ZnT3* (ZnT3$^{-/-}$/Syn-Cre^{-}/BDNF$^{flox/wt}$ or ZnT3$^{-/-}$/Syn-Cre^{-}/BDNF$^{flox/flox}$), 25% are heterozygous for the BDNF allele (ZnT3$^{-/-}$/Syn-Cre^{+}/BDNF$^{flox/wt}$), and 25% are *ZnT3/BDNF* double knockouts, henceforth referred to as ZnT3$^{-/-}$ BDNF$^{-/-}$ mice. Double mutant animals were always compared to mice that were single knockouts for either *BDNF* or *ZnT3*, referred to in this context as ZnT3$^{+/+}$ BDNF$^{-/-}$ (ZnT3$^{+/+}$/Syn-Cre^{+}/BDNF$^{flox/flox}$) or ZnT3$^{-/-}$ BDNF$^{+/+}$ (ZnT3$^{-/-}$/Syn-Cre^{-}/BDNF$^{flox/wt}$ or ZnT3$^{-/-}$/Syn-Cre^{-}/BDNF$^{flox/flox}$) animals.

All mice used in experiments were 3–6 months of age. Genotypes were confirmed by PCR at least twice. Comparisons of $BDNF^{+/+}$ with $BDNF^{-/-}$ and of $ZnT3^{-/-}$ $BDNF^{+/+}$ with $ZnT3^{-/-}$ $BDNF^{-/-}$ were performed with littermates. Comparisons of $ZnT3^{+/+}$ with $ZnT3^{-/-}$ were performed with littermate controls in some experiments and with age-matched controls (within 1.5 months of age of one another) in others; similar results were obtained with both strategies. Comparisons of $ZnT3^{+/+}$ $BDNF^{-/-}$ with $ZnT3^{-/-}$ $BDNF^{-/-}$ utilized age-matched controls.

Preparation of Brain Specimens for Immunohistochemistry

Animals were anesthetized with pentobarbital (100 mg/kg, IP) (Lundbeck, Deerfield, IL) and perfused through the left ventricle for one minute at a rate of 10 ml/min with a solution of ice-cold PBS, pH 7.4, containing 1 U/mL heparin (Sigma, St. Louis, MO) and 2 mM sodium orthovanadate (Sigma). Mice were then perfused for seven minutes with an ice-cold solution of 4% paraformaldehyde (Sigma) and 2 mM sodium orthovanadate in PBS, pH 7.4. Brains were extracted and underwent postfixation at 4°C overnight in the same solution, following which they were cryoprotected for approximately 36 hours at 4°C in a solution of 30% sucrose and 2 mM sodium orthovanadate in PBS, pH 7.4. Brains were deemed to have achieved appropriate cryoprotection upon sinking in this solution. They were then frozen by slow immersion in 2-methylbutane (J.T. Baker, Phillipsburg, NJ) which had been cooled to −20°C using dry ice. Brains were stored at −80°C until cryosectioning, at which time they were sectioned at 40 μm thickness, placed in cryoprotection solution, and again stored at −80°C until immunohistochemistry was to be performed.

Antibody Characterization

Table 1 (Primary Antibodies) and Table 2 (Secondary Antibodies) provide the details of antibodies used in this study. The peptide LQNLAKASPVpYLDI, corresponding to amino acids 806–819 of mouse TrkB receptor, was used to generate a rabbit polyclonal antibody recognizing phosphorylated tyrosine residue 816 (pY816) of TrkB. Following IgG purification with protein-A beads, this antibody was used at a 1:2000 dilution for all experiments. Importantly, the specificity of this antibody was previously established by demonstrating a significant reduction in immunoreactivity in stratum lucidum of genetically modified mice with a substitution of phenylalanine for tyrosine at the 816 residue (Y816F) of TrkB compared to wild type controls, as shown in Supplementary Figure 1 of (He et al. 2010).

Mouse monoclonal antibodies recognizing synapsin-1 (1:500; Synaptic Systems, Goettingen, Germany, Cat# 106 011, RRID:AB_887805) and tau (1:1000; Millipore, Temecula, CA, Cat# MAB3420, RRID:AB_94855) were employed for colocalization experiments. Tau antibody is a specific marker of axons (Huber and Matus, 1984), and this particular antibody was previously found to colocalize with mossy fiber axons of dentate granule cells in a transgenic line of mice expressing GFP in a subset of these neurons (Feng et al., 2000; Helgager et al., 2013). The synapsin-1 antibody used in this study has previously been employed for immunohistochemistry as a synaptic marker (Armstrong et al., 2006). Staining revealed punctate immunoreactivity within stratum lucidum, and colocalization studies further demonstrated immunoreactivity within giant mossy fiber

boutons of dentate granule cells in GFP-expressing mice, confirming synaptic labeling (data not shown).

Immunohistochemistry

Mice of the genotypes to be compared in a given experiment were always incubated in parallel using the same solutions and conditions. All incubations were performed in 5% normal goat serum (Invitrogen, Carlsbad, CA) in PBS at 4°C, pH 7.4, in the presence of 2 mM sodium orthovanadate. Floating sections were incubated for one hour in 0.5% Triton-X100 (GE Healthcare, Chalfont St. Giles, UK) for permeabilization, followed by primary antibody solutions for 36 hours. Six hour incubations with Alexa Fluor 555 goat anti-rabbit (1:1000; Invitrogen, Cat# A-21429, RRID:AB_141761) and, for experiments involving colocalization, Alexa Fluor 488 or 633 goat-anti-mouse secondary antibodies (1:500; Invitrogen, Cat# A-11029, RRID:AB_138404 and Cat# A-21052, RRID:AB_141459) then occurred. For each animal, sections not incubated with primary antibody were run in parallel as a negative control. Sections were wet-mounted on Superfrost Plus slides (Erie Scientific, Portsmouth, NH), allowed to dry onto the slides, and incubated in serial dehydration solutions for two minutes each of 50%, 70%, 85%, 95%, 100%, and 100% ethanol, followed by a 20 minute incubation in xylene (VWR, Radnor, PA) and coverslipping.

Confocal Microscopy and Data Analysis

Imaging Parameters—A Leica (Nussloch, Germany) DMIRE2 inverted microscope equipped with 10× (numerical aperture, 0.4) air and 63× (numerical aperture, 1.4) oil immersion objectives and outfitted with a Leica TCS SL confocal system was used for imaging. The pinhole was set to 1.0 Airy units for all image acquisition. All images used for quantitative analysis or shown for visual comparison between genotypes were acquired so as to prevent the introduction of artificial differences in image intensities. To this end, sections from mice which were incubated together within a given staining experiment were imaged using the same confocal settings during the same imaging session. This allowed for relative densitometry measurements to be taken between animals of different groups. Because overall staining intensities varied between experiments, settings were calibrated optimally for any given experiment so that image intensities were within the dynamic range of detection of the confocal.

Low power (10× objective, total of 100× magnification) micrographs of hippocampus are composed of average projections of *z*-series “stacks” taken through the full thickness of the section. High power (63× objective, total of 630× magnification) micrographs are average projections of *z*-series of 1 μm total thickness where pY816 staining was determined to be of greatest intensity. Average projections were used as they most accurately reflect representative staining intensities in the *z*-plane and are therefore also best for the purposes of quantification. Images demonstrating colocalizations were always confirmed in the *x*, *y*, and *z* dimensions. *Z* resolution is stated to be 235 nm (Leica) for the 63× objective used in this study, assuming ideal conditions with 488 nm light. The *x*–*y* plane resolution is stated to be 180 nm (Leica). All image quantification was performed on raw, unenhanced images. However, brightness and/or contrast were optimized in figures shown within this manuscript

so as to best convey relevant features. Brightness and contrast were adjusted equally between images meant for comparison.

Quantification of pY816 Immunoreactivity within Stratum Lucidum of Hippocampus—An investigator blinded to animal genotype performed all data analysis. ImageJ (Abramoff, 2004, http://imagej.nih.gov/ij/, RRID:nif-0000-30467) software was employed for this purpose. All quantitative data are presented as mean ± SEM, analyzed by Student's t-test.

Quantification of pY816 immunoreactivity within stratum lucidum was performed using images acquired at high power (630×). Hippocampal images including the CA3b regions of stratum lucidum and stratum radiatum were acquired bilaterally, for a total of two images per animal. Quantification focused on specific areas within stratum lucidum shown to correspond to axon tracts (Helgager et al., 2013) which were enhanced in pY816 immunoreactivity. Areas enriched in pY816 immunoreactivity were outlined as regions of interest (ROIs) until at least 40,000 pixels in total area were reached in a given image, and the average intensity of this area was quantified. The average intensity of stratum radiatum of CA3 that was included in the same image was also analyzed, and subtracted from the stratum lucidum value in order to compensate for background staining variation. This procedure was performed for images acquired from each hippocampus in a given animal, and the results averaged to yield one value per animal. Signal within stratum radiatum was used to normalize for overall staining intensity because signal within stratum radiatum was always lower than stratum lucidum, was found to be of approximately the same average intensity when compared between animals of different genotypes (data not shown), and the CA3 pyramidal cell dendrites within this region do not to contain significant levels of pY816 immunoreactivity.

Quantification of synaptic pY816 immunoreactivity within stratum lucidum utilized a synapsin-1 antibody, a specific marker of synapses (De Camilli et al., 1983; Fletcher et al., 1991; Moore and Bernstein, 1989), as described above. Z-series were acquired at 200 nm intervals over a total depth of 1 μm at 1.7× digital zoom, with three images taken per hippocampus, yielding a total of six images per animal. Individual synapsin-1 puncta were checked for pY816 immunoreactivity in the *x*, *y*, and *z* planes, and scored as being positive if they appeared to contain at least one discrete immunoreactive puncta occupying at least 20% of the area of a bouton, even if only in one *z*-section. 50 puncta were quantified per image, with a total of 300 synapsin-1 puncta per animal, and the percent of synapsin-1 puncta found to colocalize with pY816 computed.

Preparation of Brain Specimens for Western Blot and ELISA

Mice were deeply anesthetized (pentobarbital 100 mg/kg IP), following which they were decapitated and the head briefly dipped in liquid nitrogen three times. Both hippocampi were dissected on ice and placed into ice cold lysis buffer (137 mM NaCl [Sigma], 20 mM Tris [pH 7.6; Merck, Whitehouse Station, NJ], 1% NP40 [Sigma], 10% glycerol [Merck], 1 mM PMSF [Sigma], 2 mM sodium orthovanadate, and a Complete Mini protease inhibitor tablet [Roche, New Mannheim, Germany]). The hippocampi were homogenized and

centrifuged at 4°C at 14,000 RPM. For Western blot, samples were diluted to a final concentration of 1 mg/mL using lysis buffer and SDS-PAGE sample buffer (350 mM Tris [pH 6.8], 30% glycerol, 1% SDS [Crystalgen, Plainview, NY], 6% β-mercaptoethanol [Sigma], and 0.2 mg/mL bromophenol blue [Sigma]). For ELISA, acid treatment will increase yield of BDNF (Okragly and Haak-Frendscho, 1997). Therefore, the pH of the sample was adjusted to <3.0 with 1N HCl for 20 minutes at room temperature, after which it was placed on ice and brought to a pH of approximately 7.0 using 1N NaOH. Samples were then diluted to a concentration of 2.5 mg/mL using the Block & Sample buffer provided with the BDNF E_{max}® ImmunoAssay System (Promega, Madison, WI, Cat# G7611) for loading into the ELISA assay (see below).

Western Blot

Samples previously prepared for Western blot were loaded onto SDS-PAGE gels (Bio-Rad, Hercules, CA), electrophoresed, and transferred onto nitrocellulose membranes (Whatman, Dassel, Germany). After blocking in 5% bovine serum albumin (Sigma) in Tris buffered saline (TBS), membranes were incubated with primary antibodies probing for TrkB (1:2000; Chemicon, Temecula, CA, Cat# AB5372, RRID:AB_91817) or β-actin (rabbit polyclonal, 1:5000; Sigma, Cat# A2066, RRID:AB_476693). Membranes were then incubated with peroxidase conjugated goat anti-rabbit IgG secondary antibody (1:5000; The Jackson Laboratory, Cat# 111-035-006, RRID:AB_2313586), probed using ECL™ Western Blotting Analysis System (GE Healthcare, Pittsburgh, PA), and imaged in the dark on Biomax MR film (Kodak, Rochester, NY).

BDNF ELISA

The BDNF E_{max}® ImmunoAssay System, a sandwich ELISA assay, was used to measure hippocampal BDNF levels. In brief, a 96-well plate was coated with monoclonal mouse antibody (1:1000) overnight at 4°C. Samples prepared for ELISA as described above were incubated in the wells for two hours at room temperature. This was followed by incubation with a chicken polyclonal antibody recognizing BDNF (1:500) for another two hours, after which incubation with a peroxidase conjugated, anti-IgY secondary antibody (1:200) took place for one hour. TMB One Solution provided was then added to allow for color development, and the reaction was terminated with an equal volume of 1N HCl after ten minutes. A SpectraMax 190 Absorbance Microplate Reader (Molecular Devices, Sunnyvale, CA) was used to record absorbance of the wells at 450 nm. The average BDNF concentration (pg/mL) was calculated for each sample based on this absorbance reading using comparison to a standard curve, and these values were then converted to ng of BDNF per gram of total protein (ng/g).

RESULTS

Decreased Axonal and Synaptic pY816 Immunoreactivity within Stratum Lucidum in $BDNF^{-/-}$ Mice

Initial studies examined the contribution of the canonical TrkB ligand, BDNF, to activation of TrkB within stratum lucidum of hippocampus. To this end, pY816 immunoreactivity was assayed within stratum lucidum in BDNF wild type ($BDNF^{+/+}$) and knockout ($BDNF^{-/-}$)

mice using confocal microscopy. Analysis centered on the cellular and synaptic structures within stratum lucidum known to be enriched in pY816—axons and synapses of mossy fibers (Helgager et al. 2013).

Survey of the hippocampus at low power (100×) in wild type animals revealed pY816 immunoreactivity to be particularly abundant within stratum lucidum (Fig. 1A; Supplementary Fig. 1A), confirming previous results (Helgager et al. 2013). High power (630×) images revealed discrete pY816 immunoreactive patches which colocalized with tau protein (Fig. 1B–D; Supplementary Fig. 1B–D), a marker of axons, showing that this pY816 immunoreactivity corresponded anatomically to mossy fibers (Binder et al., 1985). Notably, reductions of stratum lucidum immunoreactivity were evident in $BDNF^{-/-}$ compared to $BDNF^{+/+}$ mice at low power (Fig. 2A, B), a pattern due to decreased axonal pY816 immunoreactivity within mossy fibers of $BDNF^{-/-}$ animals as detected in high magnification images (Fig. 2C, D). To quantify this reduction, high power images of stratum lucidum were acquired from both hippocampi in $BDNF^{+/+}$ (n=14) and $BDNF^{-/-}$ (n=10) littermates, and axons measured for the intensity of their immunoreactivity. Quantification revealed a reduction of pY816 immunoreactivity of approximately 30% in $BDNF^{-/-}$ compared to $BDNF^{+/+}$ animals (Fig. 2E, $p<0.05$, Student's t-test). To examine synaptic immunoreactivity, an antibody labeling the synaptic marker synapsin-1 was employed and assessed for colocalization with pY816 (De Camilli et al., 1983; Fletcher et al., 1991; Moore and Bernstein, 1989). As expected, in wild type animals a minority of synapsin-1 puncta contained pY816 immunoreactivity, also punctate in nature (Fig. 1E–J; Supplementary Fig. 1E–J). To quantify synaptic immunoreactivity in $BDNF^{+/+}$ (n=9) and $BDNF^{-/-}$ (n=6) mice, synapsin-1 puncta were identified in *z*-section stacks and scored for pY816 immunoreactivity by a blinded investigator (4500 synapsin-1 puncta total). In $BDNF^{+/+}$ animals, an average of 17.4 ± 1.1% of synapsin-1 puncta were found to contain pY816 immunoreactivity, whereas only 13.3 ± 1.0% contained pY816 in the $BDNF^{-/-}$ mouse, a statistically significant reduction (Fig. 2F, mean ± SEM, $p<0.05$ by Student's t-test). The reductions of pY816 immunoreactivity within both axons and boutons of mossy fibers support the conclusion that BDNF contributes to TrkB activation under these conditions.

pY816 TrkB Immunoreactivity within Stratum Lucidum of $ZnT3^{-/-}$ Mice

To assess the contribution of vesicular zinc to activation of TrkB within stratum lucidum of hippocampus, pY816 immunoreactivity was examined in hippocampal sections from mice in which the transporter required for concentrating zinc within synaptic vesicles (ZnT3) had been eliminated. Synaptic immunoreactivity was assayed in the same fashion as was performed in the BDNF knockout animals above, with over 11,500 synapsin-1 puncta examined in $ZnT3^{+/+}$ (n=19) and $ZnT3^{-/-}$ (n=19) animals. No significant differences in the percentages of pY816+ synapses were detected between the two genotypes (Fig. 3F; $ZnT3^{+/+}$ = 17.5 ± 0.9%, $ZnT3^{-/-}$ = 17.1 ± 0.9%, mean % ± SEM, p=0.77 by Student's t-test). Unexpectedly, inspection of stratum lucidum from $ZnT3^{-/-}$ mice revealed *increased* pY816 immunoreactivity within this region compared to the $ZnT3^{+/+}$ animal (Fig. 3A–D). High power micrographs revealed colocalization of pY816 immunoreactivity with tau in the ZnT3 mutant as observed in WT, confirming localization within axons of mossy fibers (data not shown). Quantification of axonal immunoreactivity in $ZnT3^{+/+}$ (n=19) and $ZnT3^{-/-}$

(n=19) animals revealed an increase of pY816 immunoreactivity approximating 24% in the ZnT3 knockout mouse compared to wild type (Fig. 3E; $p<0.01$ by Student's t-test).

Total TrkB Levels Are Unchanged in Hippocampi of ZnT3$^{-/-}$ Mice

The increases observed in pY816 immunoreactivity within mossy fiber axons in the *ZnT3* knockout animal could be due to increased numbers of TrkB molecules in ZnT3$^{-/-}$ compared to ZnT3$^{+/+}$ controls, a similar proportion of which are phosphorylated. Such a finding would reflect one potential molecular mechanism leading to increased pY816 in the absence of vesicular zinc. Alternatively, the numbers of TrkB molecules could be equivalent in ZnT3$^{-/-}$ compared to ZnT3$^{+/+}$ controls, but a greater proportion could be phosphorylated in the mutant compared to wild type. To begin to assess these possibilities, Western blots were performed on hippocampal lysates from ZnT3$^{+/+}$ and ZnT3$^{-/-}$ animals, probing for the TrkB receptor (Fig. 4A). Quantification of wild type (n=13) and knockout (n=11) animals revealed no overt differences in TrkB receptor levels between these two genotypes (Fig. 4B; $p=0.64$ by Student's t-test).

BDNF Levels Increase within Hippocampi of ZnT3$^{-/-}$ Mice

The unexpected increase of axonal pY816 immunoreactivity together with the lack of change in TrkB protein levels was consistent with enhanced activation of TrkB, raising the possibility of an increase in expression of the canonical TrkB ligand, BDNF, in the *ZnT3* mutant mouse. To examine this possibility, BDNF content was measured in hippocampal lysates isolated from ZnT3$^{+/+}$ (n=10) and ZnT3$^{-/-}$ (n=8) animals using an ELISA. This revealed a 51% increase in BDNF content (ZnT3$^{+/+}$ = 81 ± 9 pg/g, ZnT3$^{-/-}$ = 123 ± 10 pg/g, mean pg BDNF/g total protein ± SEM, $p<0.01$ by Student's t-test) in ZnT3$^{-/-}$ compared to ZnT3$^{+/+}$ mice (Fig. 4C).

Axonal and Synaptic pY816 TrkB Immunoreactivity within Stratum Lucidum Is Reduced in ZnT3$^{-/-}$ BDNF$^{-/-}$ Compared to ZnT3$^{-/-}$ BDNF$^{+/+}$ Mice

The increased BDNF content in *ZnT3* mutant mice led us to hypothesize that this response is required for the increased mossy fiber axonal pY816 detected in these animals. To test this hypothesis, the effects of eliminating BDNF from *ZnT3* mutant mice on pY816 immunoreactivity were examined by breeding *BDNF* mutant mice on to a *ZnT3* null mutant background (see Materials and Methods). Importantly, *ZnT3* and *BDNF* double mutant animals (ZnT3$^{-/-}$ BDNF$^{-/-}$) were behaviorally indistinguishable from wild type mice by casual observation, were born in normal Mendelian ratios, and exhibited similar body weight in comparison to their ZnT3$^{-/-}$ single knockout littermates (data not shown). Consistent with this idea, elimination of BDNF protein reduced pY816 immunoreactivity in mossy fiber axons in ZnT3$^{-/-}$ BDNF$^{-/-}$ compared to ZnT3$^{-/-}$ BDNF$^{+/+}$ littermate controls (Fig. 5A–D). Quantification of axonal pY816 immunoreactivity revealed a 36% reduction in ZnT3$^{-/-}$ BDNF$^{-/-}$ (n=10) compared to ZnT3$^{-/-}$ BDNF$^{+/+}$ (n=11) littermates (Fig. 5E, $p<0.001$ by Student's t-test). Similar results were evident with measures of pY816 immunoreactivity in mossy fiber boutons. That is, quantification of over 4800 synapsin-1 puncta revealed significant reductions of pY816 positive synapsin-1 puncta in ZnT3$^{-/-}$ BDNF$^{-/-}$ (n=8) animals compared to ZnT3$^{-/-}$ BDNF$^{+/+}$ (n=8) control mice (Fig. 5F,

$ZnT3^{-/-}$ $BDNF^{+/+}$ = 18 ± 1%, $ZnT3^{-/-}$ $BDNF^{-/-}$ = 12 ± 2%, mean % ± SEM, $p<0.05$ by Student's t-test). In sum, these findings support the hypothesis that BDNF contributes to both synaptic and axonal pY816 content in the *ZnT3* null mutant mice.

Axonal and Synaptic pY816 TrkB Immunoreactivity in Stratum Lucidum Is Not Further Reduced in $ZnT3^{-/-}$ $BDNF^{-/-}$ Compared to $ZnT3^{+/+}$ $BDNF^{-/-}$ Mice

We suspected that the increased BDNF in the hippocampi of $ZnT3^{-/-}$ mice may be a homeostatic compensation triggered by a lack of TrkB transactivation by vesicular zinc. If so, then eliminating ZnT3 from mice lacking *BDNF* would be predicted to reduce pY816 immunoreactivity. To test this idea, we compared pY816 immunoreactivity within mossy fiber axons and boutons of *BDNF* mutant mice in those wild type ($ZnT3^{+/+}$ $BDNF^{-/-}$ single knockout) and null ($ZnT3^{-/-}$ $BDNF^{-/-}$ double knockout) for ZnT3. Contrary to our prediction, no significant decreases of pY816 immunoreactivity within mossy fiber axons were detected in the double compared to single knockout animals (Fig. 6A–E; p=0.25 by Student's t-test). Likewise, no significant change in the percent of pY816 immunoreactive synapses was detected in the double knockout (n=8) compared to *BDNF* single knockout (n=6) mice (Fig. 6F; $ZnT3^{+/+}$ $BDNF^{-/-}$ = 13.3 ± 1.0%, $ZnT3^{-/-}$ $BDNF^{-/-}$ = 11.8 ± 1.6%, mean % ± SEM, p=0.49 by Student's t-test). In sum, these experiments failed to provide evidence that vesicular zinc is transactivating TrkB under physiological conditions in the adult mouse.

DISCUSSION

The goal of this study was to test the contribution of BDNF and synaptic vesicular zinc to TrkB activation within the axons and presynaptic boutons of hippocampal dentate granule cells of adult mice. To this end, we conducted immunohistochemical experiments with high resolution confocal microscopy using an antibody that probes for pY816 of TrkB in brain sections isolated from WT or genetically modified mice devoid of BDNF and/or synaptic vesicular zinc. Our previous work (Huang et al., 2008) led us to hypothesize that both BDNF and synaptic vesicular zinc would contribute to TrkB activation. Four principal findings emerged: (1) pY816 immunoreactivity is reduced in both axons and synaptic boutons of mossy fibers in mice lacking BDNF. (2) Unexpectedly, pY816 immunoreactivity was increased in mossy fiber axons of mice lacking vesicular zinc, whereas immunoreactivity within presynaptic boutons was unchanged. (3) Marked increases of BDNF content were evident within the hippocampus of mice devoid of synaptic vesicular zinc and elimination of BDNF reduced pY816 immunoreactivity in these mice. (4) In mice null for BDNF, elimination of synaptic vesicular zinc produced no significant reduction of pY816 immunoreactivity in either axons or synaptic boutons of mossy fibers. These findings support the following conclusions: (1) BDNF but not vesicular zinc promotes the activation of TrkB in the adult mouse brain under physiological conditions; and (2) Elimination of vesicular zinc evokes a homeostatic response evident by enhanced expression of BDNF which in turn promotes activation of TrkB.

The reduction of pY816 immunoreactivity within axons and boutons of mossy fibers in BDNF mutants implicates BDNF as an endogenous agonist for TrkB under physiological

conditions in adult mice. Biochemical analyses have revealed enhanced TrkB activation in adult rodent brains following a diversity of *in vivo* perturbations (Hu and Russek, 2008; Chao et al., 2006), including drugs such as cocaine (Crooks et al., 2010) and antidepressants (Saarelainen et al., 2003; Li et al., 2008) as well as insults such as traumatic brain injury (Hu et al, 2004), ischemia (Hu et al, 2000), and seizures (Yan et al., 1997; He et al., 2004; Lessmann and Brigadski, 2009). Immunohistochemical studies have also confirmed and extended these biochemical results, revealing regulation of TrkB activation with distinct stages of estrous cycle (Spencer-Segal et al., 2011) and with learning paradigms (Chen et al., 2010a; Chen et al., 2010b). While the ligand mediating TrkB activation in these diverse studies has been thought to be its canonical ligand, BDNF, we are unaware of studies directly demonstrating this *in vivo*. The present evidence implicating endogenous BDNF in TrkB activation under physiological conditions in the adult brain is consistent with behavioral observations of impaired learning and memory (Heldt et al., 2007; Linnarsson et al., 1997; Mizuno et al., 2000; Monteggia et al., 2004), impaired epileptogenesis (Kokaia et al., 1995; He et al 2004), and impaired synaptic plasticity (Figurov et al., 1996; Korte et al., 1995; Korte et al., 1996; Patterson et al., 1996; Zakharenko et al., 2003) caused by genetic or pharmacological perturbations of BDNF.

In our earlier studies, we found no significant reduction of pTrkB immunoreactivity in these same conditional BDNF knockout mice (He et al., 2004). This discrepancy is likely due to the insensitivity of the pTrkB antibody in our earlier work, precluding detection of pTrkB under physiological conditions in the adult brain. The higher resolution analysis (630× as opposed to 100×) used in the present work also enabled study of individual axons and boutons without measure of signal between these processes; measures of the entire area of stratum lucidum including regions between axons and boutons diluted the signal from these processes and failed to detect significant differences between wild type and BDNF conditional knockout mice in the present study (data not shown). Notably, the magnitude of the reduction of pY816 immunoreactivity within axons and boutons of mossy fibers in the absence of BDNF in the present study was modest (approximating 30%). Whether residual pY816 immunoreactivity is due to TrkB activation by another neurotrophin, such as NT4, and/or transactivation by a non-neurotrophin stimulus, requires further investigation.

The present findings are consistent with a model in which endogenous BDNF is packed within dense-core vesicles and released from mossy fiber boutons under physiological conditions. Following release, it binds to the ectodomain of TrkB in the synaptic membrane of the same or nearby terminals in an autocrine or paracrine fashion, and is subsequently endocytosed (Senger and Campenot, 1997; Bhattacharyya et al., 1997; Dieni et al, 2012). We favor the mossy fibers of the dentate granule cells as the cellular source of BDNF that activates TrkB because of the immunohistochemical evidence of high levels of BDNF protein in giant boutons of the mossy fibers (Danzer and McNamara, 2004; Yan et al., 1997). Within these boutons BDNF is likely to be located within dense core vesicles (Dieni et al., 2012). By contrast, immunohistochemical studies failed to detect BDNF protein in dendrites of CA3 pyramidal cells (Danzer and McNamara, 2004; Dieni et al., 2012; Yan et al., 1997). It should be noted, however, that a small fraction of dendritic spines of CA3 pyramidal cells within stratum lucidum were found to be immunoreactive for BDNF

(Danzer and McNamara, 2004), raising the possibility of a dendritic source of BDNF contributing to the activation of TrkB on presynaptic terminal membranes of mossy fiber axons (Baj et al., 2011; Chiaruttini et al., 2009; Tongiorgi et al., 2004).

The idea that pTrkB immunoreactivity detected within boutons in this study appears to be localized to small organelles is consistent with its undergoing endocytosis following activation at the membrane of the presynaptic terminal. The established model of retrograde transport of nerve growth factor-activated TrkA based upon studies of the peripheral nervous system raises the possibility that the pTrkB within mossy fiber axons may be en route from the presynaptic terminals to the granule cell bodies (Bhattacharyya et al., 1997; Niewiadomska et al., 2011; Watson et al., 1999). Alternatively, the pTrkB in mossy fiber axons may reflect locally processed TrkB following its activation (Senger and Campenot, 1997; Bhattacharyya et al., 1997; Dieni et al, 2012); the absence of detectable pY816 immunoreactivity in granule cell bodies favors this latter possibility (data not shown). Electrophysiological studies reveal that one biological consequence of BDNF-mediated TrkB activation locally within mossy fiber boutons may be a form of LTP of the mossy fiber-CA3 synapse that is presynaptic in both its induction and expression (Huang et al., 2008; Pan et al., 2011).

The primary objective of these experiments was to test the hypothesis that synaptic vesicular zinc transactivates TrkB under physiological conditions in the adult mouse. This hypothesis predicts that elimination of synaptic vesicular zinc in a mouse lacking BDNF would further reduce pY816 immunoreactivity. Contrary to our hypothesis, elimination of vesicular zinc induced no further reduction of pY816 immunoreactivity in either axons or boutons of dentate granule cells when compared to the absence of BDNF alone. In contrast to the predicted reduction, elimination of synaptic vesicular zinc in WT mice produced an increase, not decrease, of pY816 immunoreactivity in axons of dentate granule cells. We suspect that this increase in pY816 immunoreactivity is due to a homeostatic increase of BDNF expression, a suspicion supported by both the increased BDNF content in mice lacking vesicular zinc and the reduction of pY816 immunoreactivity when BDNF was eliminated from ZnT3 knockout animals. The mechanism by which depletion of vesicular zinc induces a homeostatic increase of BDNF is not clear. Removal of vesicular zinc-mediated inhibition of the NMDA receptor component of the mossy fiber-evoked EPSC in CA3 pyramidal cells (Pan et al., 2012) may contribute to the increased BDNF in ZnT3 mutant mice; this is because NMDA receptor activation can promote increases of BDNF content (Vanhoutte and Bading, 2003). An alternative possibility, a requirement of vesicular zinc for protease cleavage of pro- to mature BDNF, is unlikely as this mechanism predicts a decrease in BDNF in mice lacking vesicular zinc (Hwang et al., 2005).

The homeostatic response of BDNF and TrkB activation in the absence of synaptic vesicular zinc notwithstanding, our results provide no evidence that vesicular zinc mediates activation of TrkB *in vivo*. *In vitro* experiments demonstrate that application of exogenous zinc to cultured cells can activate TrkB in the absence of neurotrophins including BDNF (Huang et al 2008). The zinc-dependence of depolarization-induced increases of TrkB activation in cultured neurons suggests that synaptic vesicular zinc is one pool of endogenous zinc mediating transactivation. That said, the observation of enhanced activation of TrkB

occurring in the mossy fiber pathway in mice lacking BDNF was made following seizures induced *in vivo* (He et al 2004). While the peak concentration of zinc in the synaptic cleft induced by high frequency firing of mossy fibers is thought to approximate 100 μM (Vogt et al 2000; Pan et al 2011), the concentration under physiological conditions is likely to be at least 10–100 fold lower. Examining the effects of various concentrations of exogenous zinc on TrkB activation in cultured neurons revealed small increases at 2 μM with the most robust increases at concentrations of 20–100 μM (Huang et al 2008). We suspect that the low concentrations of zinc in the synaptic cleft under physiological conditions *in vivo* in the present experiments failed to induce sufficient activation of TrkB to be detectable. Whether vesicular zinc can transactivate TrkB *in vivo* under seizure conditions—when high frequency firing of mossy fibers results in higher concentrations of zinc within the synaptic cleft—remains to be determined.

In sum, the present findings support the conclusion that the dominant ligand mediating activation of TrkB under physiological conditions in the adult mouse brain is the neurotrophin BDNF. Contrary to our hypothesis derived from *in vitro* studies (Huang et al 2008), no evidence was found that synaptic vesicular zinc transactivates the TrkB receptor under these conditions, though it remains to be tested whether this ligand contributes to TrkB activation under different circumstances, such as during seizures. The enhanced activation of TrkB induced by elimination of vesicular zinc in the present experiments is mediated indirectly by BDNF, a mechanism distinct from transactivation.

Supplementary Material

Refer to Web version on PubMed Central for supplementary material.

Acknowledgments

Support

This work was supported by a grant from NINDS NS065960 (J.O.M), The Wakeman Endowment through the Wakeman Award at Duke University (J.H.), and a Taking Flight Award from the CURE foundation (Y.Z.H.).

OTHER ACKNOWLEDGEMENTS

The authors wish to strongly acknowledge Wei-Hua Qian for her assistance with mouse genotyping and husbandry.

LITERATURE CITED

Abramoff MD, Magelhaes PJ, Ram SJ. Image Processing with ImageJ. Biophotonics International. 2004; 11(7):36–42.

Armstrong JN, Saganich MJ, Xu NJ, Henkemeyer M, Heinemann SF, Contractor A. B-ephrin reverse signaling is required for NMDA-independent long-term potentiation of mossy fibers in the hippocampus. J Neurosci. 2006; 26(13):3474–3481. [PubMed: 16571754]

Baj G, Leone E, Chao MV, Tongiorgi E. Spatial segregation of BDNF transcripts enables BDNF to differentially shape distinct dendritic compartments. Proc Natl Acad Sci U S A. 2011; 108(40): 16813–16818. [PubMed: 21933955]

Barbacid M. Neurotrophic factors and their receptors. Curr Opin Cell Biol. 1995; 7(2):148–155. [PubMed: 7612265]

Bhattacharyya A, Watson FL, Bradlee TA, Pomeroy SL, Stiles CD, Segal RA. Trk receptors function as rapid retrograde signal carriers in the adult nervous system. J Neurosci. 1997; 17(18):7007–7016. [PubMed: 9278536]

Binder LI, Frankfurter A, Rebhun LI. The distribution of tau in the mammalian central nervous system. J Cell Biol. 1985; 101(4):1371–1378. [PubMed: 3930508]

Carpenter G. Employment of the epidermal growth factor receptor in growth factor-independent signaling pathways. J Cell Biol. 1999; 146(4):697–702. [PubMed: 10459005]

Chao MV, Rajagopal R, Lee FS. Neurotrophin signalling in health and disease. Clin Sci (Lond). 2006; 110(2):167–173. [PubMed: 16411893]

Chen LY, Rex CS, Pham DT, Lynch G, Gall CM. BDNF signaling during learning is regionally differentiated within hippocampus. J Neurosci. 2010a; 30(45):15097–15101. [PubMed: 21068315]

Chen LY, Rex CS, Sanaiha Y, Lynch G, Gall CM. Learning induces neurotrophin signaling at hippocampal synapses. Proc Natl Acad Sci U S A. 2010b; 107(15):7030–7035. [PubMed: 20356829]

Chiaruttini C, Vicario A, Li Z, Baj G, Braiuca P, Wu Y, Lee FS, Gardossi L, Baraban JM, Tongiorgi E. Dendritic trafficking of BDNF mRNA is mediated by translin and blocked by the G196A (Val66Met) mutation. Proc Natl Acad Sci U S A. 2009; 106(38):16481–16486. [PubMed: 19805324]

Choi DW, Koh JY. Zinc and brain injury. Annual review of neuroscience. 1998; 21:347–375.

Cole TB, Wenzel HJ, Kafer KE, Schwartzkroin PA, Palmiter RD. Elimination of zinc from synaptic vesicles in the intact mouse brain by disruption of the ZnT3 gene. Proc Natl Acad Sci U S A. 1999; 96(4):1716–1721. [PubMed: 9990090]

Cunningham ME, Greene LA. A function-structure model for NGF-activated TRK. Embo J. 1998; 17(24):7282–7293. [PubMed: 9857185]

Danzer SC, McNamara JO. Localization of brain-derived neurotrophic factor to distinct terminals of mossy fiber axons implies regulation of both excitation and feedforward inhibition of CA3 pyramidal cells. J Neurosci. 2004; 24(50):11346–11355. [PubMed: 15601941]

De Camilli P, Harris SM Jr, Huttner WB, Greengard P. Synapsin I (Protein I), a nerve terminal-specific phosphoprotein. II. Its specific association with synaptic vesicles demonstrated by immunocytochemistry in agarose-embedded synaptosomes. J Cell Biol. 1983; 96(5):1355–1373. [PubMed: 6404911]

Dieni S, Matsumoto T, Dekkers M, Rauskolb S, Ionescu MS, Deogracias R, Gundelfinger ED, Kojima M, Nestel S, Frotscher M, Barde YA. BDNF and its pro-peptide are stored in presynaptic dense core vesicles in brain neurons. J Cell Biol. 2012; 196(6):775–788. [PubMed: 22412021]

Feng G, Mellor RH, Bernstein M, Keller-Peck C, Nguyen QT, Wallace M, Nerbonne JM, Lichtman JW, Sanes JR. Imaging neuronal subsets in transgenic mice expressing multiple spectral variants of GFP. Neuron. 2000; 28(1):41–51. [PubMed: 11086982]

Figurov A, Pozzo-Miller LD, Olafsson P, Wang T, Lu B. Regulation of synaptic responses to high-frequency stimulation and LTP by neurotrophins in the hippocampus. Nature. 1996; 381(6584): 706–709. [PubMed: 8649517]

Fletcher TL, Cameron P, De Camilli P, Banker G. The distribution of synapsin I and synaptophysin in hippocampal neurons developing in culture. J Neurosci. 1991; 11(6):1617–1626. [PubMed: 1904480]

Frederickson CJ, Danscher G. Zinc-containing neurons in hippocampus and related CNS structures. Progress in brain research. 1990; 83:71–84. [PubMed: 2203108]

Frederickson CJ, Koh JY, Bush AI. The neurobiology of zinc in health and disease. Nature reviews Neuroscience. 2005; 6(6):449–462.

Gu H, Marth JD, Orban PC, Mossmann H, Rajewsky K. Deletion of a DNA polymerase beta gene segment in T cells using cell type-specific gene targeting. Science. 1994; 265(5168):103–106. [PubMed: 8016642]

He XP, Kotloski R, Nef S, Luikart BW, Parada LF, McNamara JO. Conditional deletion of TrkB but not BDNF prevents epileptogenesis in the kindling model. Neuron. 2004; 43(1):31–42. [PubMed: 15233915]

Heldt SA, Stanek L, Chhatwal JP, Ressler KJ. Hippocampus-specific deletion of BDNF in adult mice impairs spatial memory and extinction of aversive memories. Mol Psychiatry. 2007; 12(7):656–670. [PubMed: 17264839]

Helgager J, Liu G, McNamara JO. The cellular and synaptic location of activated TrkB in mouse hippocampus during limbic epileptogenesis. J Comp Neurol. 2013; 521(3):499–521. [PubMed: 22987780]

Huang EJ, Reichardt LF. Neurotrophins: roles in neuronal development and function. Annual review of neuroscience. 2001; 24:677–736.

Huang YZ, Pan E, Xiong ZQ, McNamara JO. Zinc-mediated transactivation of TrkB potentiates the hippocampal mossy fiber-CA3 pyramid synapse. Neuron. 2008; 57(4):546–558. [PubMed: 18304484]

Huber G, Matus A. Differences in the cellular distributions of two microtubule-associated proteins, MAP1 and MAP2, in rat brain. J Neurosci. 1984; 4(1):151–160. [PubMed: 6198491]

Korte M, Carroll P, Wolf E, Brem G, Thoenen H, Bonhoeffer T. Hippocampal long-term potentiation is impaired in mice lacking brain-derived neurotrophic factor. Proc Natl Acad Sci U S A. 1995; 92(19):8856–8860. [PubMed: 7568031]

Korte M, Griesbeck O, Gravel C, Carroll P, Staiger V, Thoenen H, Bonhoeffer T. Virus-mediated gene transfer into hippocampal CA1 region restores long-term potentiation in brain-derived neurotrophic factor mutant mice. Proc Natl Acad Sci U S A. 1996; 93(22):12547–12552. [PubMed: 8901619]

Linnarsson S, Bjorklund A, Ernfors P. Learning deficit in BDNF mutant mice. Eur J Neurosci. 1997; 9(12):2581–2587. [PubMed: 9517463]

McAllister AK, Katz LC, Lo DC. Neurotrophins and synaptic plasticity. Annual review of neuroscience. 1999; 22:295–318.

McNamara JO, Huang YZ, Leonard AS. Molecular signaling mechanisms underlying epileptogenesis. Sci STKE. 2006; 2006(356):re12. [PubMed: 17033045]

Mizuno M, Yamada K, Olariu A, Nawa H, Nabeshima T. Involvement of brain-derived neurotrophic factor in spatial memory formation and maintenance in a radial arm maze test in rats. J Neurosci. 2000; 20(18):7116–7121. [PubMed: 10995859]

Monteggia LM, Barrot M, Powell CM, Berton O, Galanis V, Gemelli T, Meuth S, Nagy A, Greene RW, Nestler EJ. Essential role of brain-derived neurotrophic factor in adult hippocampal function. Proc Natl Acad Sci U S A. 2004; 101(29):10827–10832. [PubMed: 15249684]

Moore RY, Bernstein ME. Synaptogenesis in the rat suprachiasmatic nucleus demonstrated by electron microscopy and synapsin I immunoreactivity. J Neurosci. 1989; 9(6):2151–2162. [PubMed: 2498469]

Niewiadomska G, Mietelska-Porowska A, Mazurkiewicz M. The cholinergic system, nerve growth factor and the cytoskeleton. Behav Brain Res. 2011; 221(2):515–526. [PubMed: 20170684]

Okragly AJ, Haak-Frendscho M. An acid-treatment method for the enhanced detection of GDNF in biological samples. Exp Neurol. 1997; 145(2 Pt 1):592–596. [PubMed: 9217096]

Pan E, Zhang XA, Huang Z, Krezel A, Zhao M, Tinberg CE, Lippard SJ, McNamara JO. Vesicular zinc promotes presynaptic and inhibits postsynaptic long-term potentiation of mossy fiber-CA3 synapse. Neuron. 2011; 71(6):1116–1126. [PubMed: 21943607]

Patterson SL, Abel T, Deuel TA, Martin KC, Rose JC, Kandel ER. Recombinant BDNF rescues deficits in basal synaptic transmission and hippocampal LTP in BDNF knockout mice. Neuron. 1996; 16(6):1137–1145. [PubMed: 8663990]

Poo MM. Neurotrophins as synaptic modulators. Nature reviews Neuroscience. 2001; 2(1):24–32.

Segal RA, Bhattacharyya A, Rua LA, Alberta JA, Stephens RM, Kaplan DR, Stiles CD. Differential utilization of Trk autophosphorylation sites. J Biol Chem. 1996; 271(33):20175–20181. [PubMed: 8702742]

Spencer-Segal JL, Waters EM, Bath KG, Chao MV, McEwen BS, Milner TA. Distribution of phosphorylated TrkB receptor in the mouse hippocampal formation depends on sex and estrous cycle stage. J Neurosci. 2011; 31(18):6780–6790. [PubMed: 21543608]

Tongiorgi E, Armellin M, Giulianini PG, Bregola G, Zucchini S, Paradiso B, Steward O, Cattaneo A, Simonato M. Brain-derived neurotrophic factor mRNA and protein are targeted to discrete

dendritic laminas by events that trigger epileptogenesis. J Neurosci. 2004; 24(30):6842–6852. [PubMed: 15282290]

Watson FL, Heerssen HM, Moheban DB, Lin MZ, Sauvageot CM, Bhattacharyya A, Pomeroy SL, Segal RA. Rapid nuclear responses to target-derived neurotrophins require retrograde transport of ligand-receptor complex. J Neurosci. 1999; 19(18):7889–7900. [PubMed: 10479691]

Yan Q, Rosenfeld RD, Matheson CR, Hawkins N, Lopez OT, Bennett L, Welcher AA. Expression of brain-derived neurotrophic factor protein in the adult rat central nervous system. Neuroscience. 1997; 78(2):431–448. [PubMed: 9145800]

Zakharenko SS, Patterson SL, Dragatsis I, Zeitlin SO, Siegelbaum SA, Kandel ER, Morozov A. Presynaptic BDNF required for a presynaptic but not postsynaptic component of LTP at hippocampal CA1-CA3 synapses. Neuron. 2003; 39(6):975–990. [PubMed: 12971897]

Zhu Y, Romero MI, Ghosh P, Ye Z, Charnay P, Rushing EJ, Marth JD, Parada LF. Ablation of NF1 function in neurons induces abnormal development of cerebral cortex and reactive gliosis in the brain. Genes Dev. 2001; 15(7):859–876. [PubMed: 11297510]

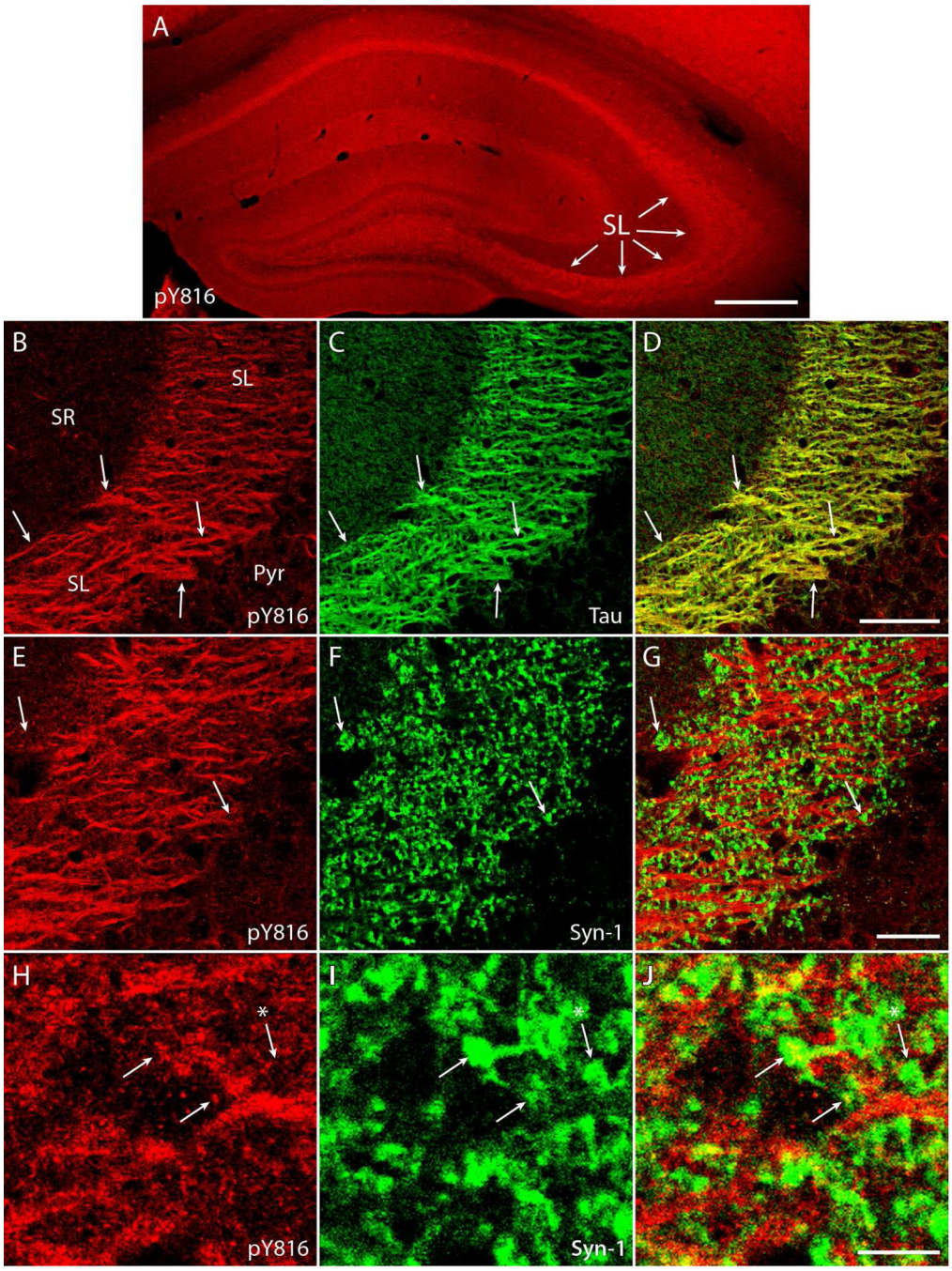

Figure 1. Immunoreactivity for phosphorylated residue 816 of the TrkB receptor (pY816) is enriched in mossy fiber axons and synapses within stratum lucidum of mouse hippocampus

A) Image of an entire mouse hippocampus in a wild type animal, stained with pY816. The stratum lucidum region (arrows) appears particularly enriched in pY816 immunoreactivity. Image is a montage of two images taken at low magnification (100×). Scale bar = 300 μm. B-D) High power (630×) images of stratum lucidum of hippocampus stained for pY816 (B, red) and tau (C, green), an axonal marker. Discrete patches of pY816 immunoreactivity (B, red; arrows) overlap with tau labeled axons (C, green; arrows), demonstrating mossy fiber axons of dentate granule cells are particularly enriched in pY816 immunoreactivity. Merged

pY816 and tau is shown in (D). SR = stratum radiatum of CA3, Pyr = CA3 pyramidal cell layer. Scale bar = 50 μm. E-G) Confocal micrographs showing stratum lucidum stained with pY816 (E, red) and synapsin-1 (F, green), a marker of synapses. The majority of synapsin-1 puncta (F, green; arrows) do not appear to contain substantial pY816 (E, red; arrows). Merged pY816 and synapsin-1 is shown in (G). Scale bar = 30 μm. H-J) Digitally zoomed images consisting of one *z*-section from images in (E–G) demonstrate synapsin-1 puncta (I, green; arrows) that contain pY816 immunoreactivity (H, red; arrows). A nearby synapsin-1 puncta (I, green; arrow with asterisk) does not contain pY816 immunoreactivity (H, red; arrow with asterisk), the situation for the majority of synapsin-1 puncta assessed. Merged pY816 and synapsin-1 is shown in (J). Scale bar = 7 μm.

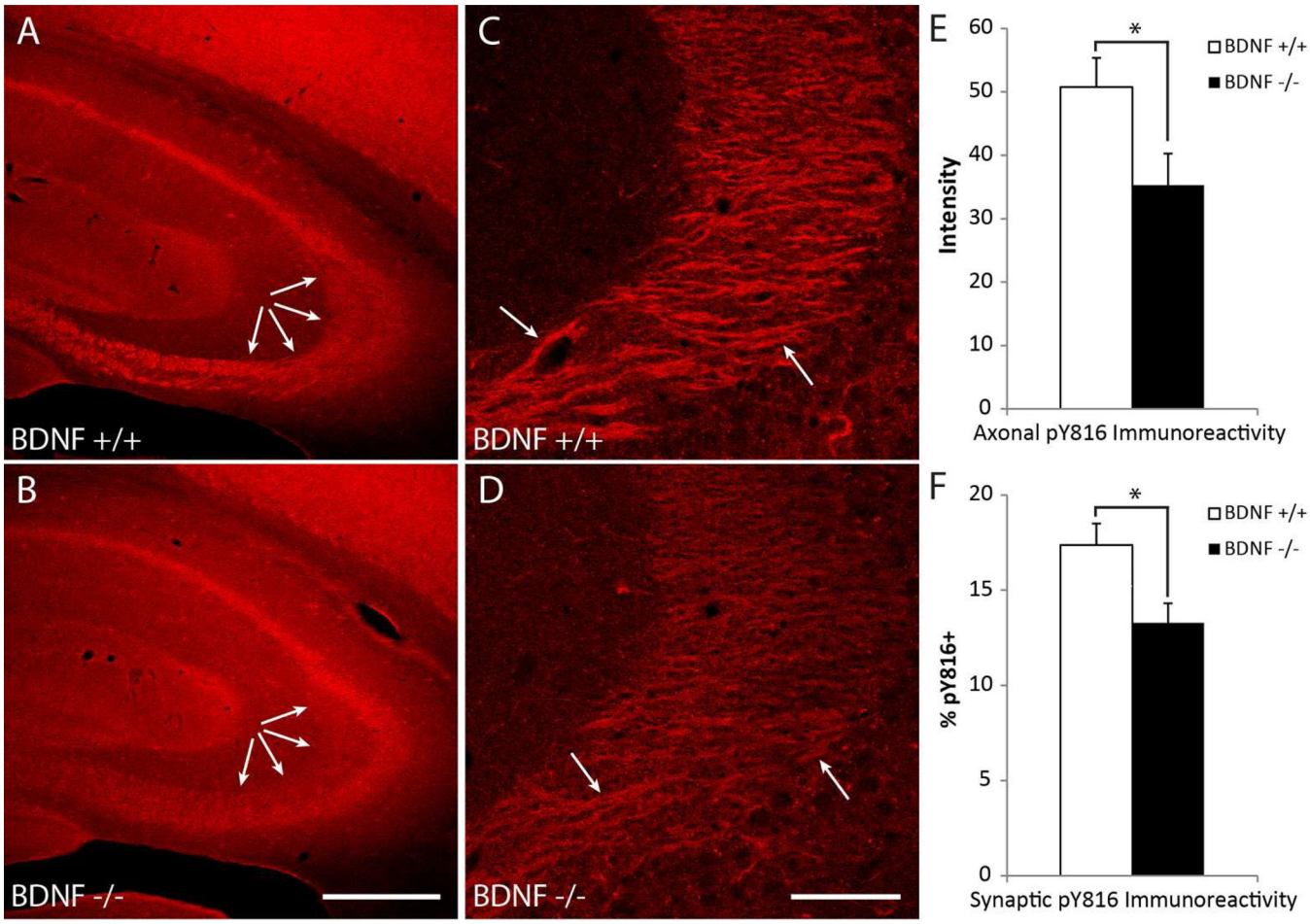

Figure 2. pY816 TrkB immunoreactivity in mossy fiber axons and synapses within stratum lucidum is decreased in brain-derived neurotrophic factor knockout ($BDNF^{-/-}$) compared to wild type ($BDNF^{+/+}$) mice

A&B) Representative low power micrographs taken of hippocampi from $BDNF^{+/+}$ (A) and $BDNF^{-/-}$ (B) mice stained with pY816, revealing that immunoreactivity within stratum lucidum of the $BDNF^{-/-}$ animal (B, arrows) is reduced compared to its $BDNF^{+/+}$ littermate (A, arrows). Scale bar = 300 μm. C&D) Images of stratum lucidum taken at high power from pY816 stained sections from the same $BDNF^{+/+}$ (C) and $BDNF^{-/-}$ (D) mice as in (A&B) demonstrates that this observed reduction is due to decreased pY816 immunoreactivity within mossy fiber axons of the $BDNF^{-/-}$ mouse (arrows point to pY816 enriched regions shown in Fig. 1 and Supplementary Fig. 1 to correspond anatomically to mossy fiber axons). Scale bar = 50 μm. E) Quantification of axonal pY816 immunoreactivity in $BDNF^{+/+}$ (n=14) and $BDNF^{-/-}$ (n=10) mice demonstrates a significant decrease in immunoreactivity in the $BDNF^{-/-}$ animal compared to $BDNF^{+/+}$ ($p<0.05$, Student's t-test). Quantification is presented as mean pY816 axonal immunoreactivity ± SEM. F) Quantification of percentages of synapsin-1 puncta within stratum lucidum found to contain pY816 immunoreactivity in $BDNF^{+/+}$ (n=9) and $BDNF^{-/-}$ (n=6) mice. A 30.8% reduction in synaptic pY816 immunoreactivity was found in $BDNF^{-/-}$ mice compared to their $BDNF^{+/+}$ littermates ($p<0.05$, Student's t-test). A total of 2700 synapsin-1 puncta were analyzed in

BDNF$^{+/+}$ mice, and 1800 in BDNF$^{-/-}$ animals. Quantification is presented as mean % ± SEM. All data were analyzed by Student's t-test; *$p<0.05$.

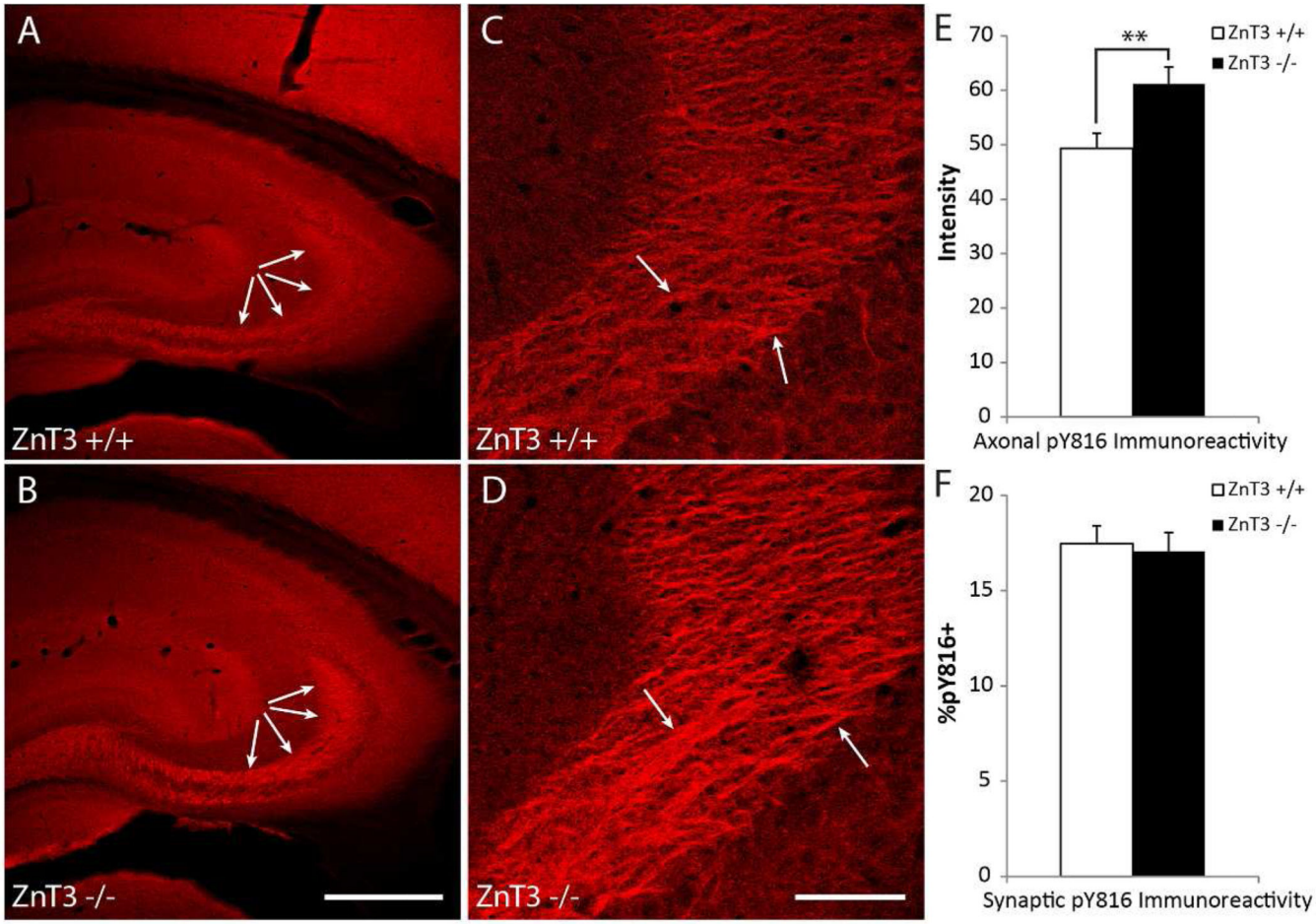

Figure 3. Axonal pY816 TrkB immunoreactivity increases in axons but remains unchanged at synapses within stratum lucidum in zinc transporter protein-3 knockout ($ZnT3^{-/-}$) compared to wild type ($ZnT3^{+/+}$) mice

A&B) Representative low power images of hippocampi stained with pY816, taken from $ZnT3^{+/+}$ (A) and $ZnT3^{-/-}$ (B) mice showing increased immunoreactivity within stratum lucidum in the $ZnT3^{-/-}$ mouse (B, arrows) compared to its $ZnT3^{+/+}$ littermate (A, arrows). Scale bar = 300 μm. C&D) High power micrographs of stratum lucidum taken from pY816 stained sections from the same $ZnT3^{+/+}$ (C) and $ZnT3^{-/-}$ (D) animals as in (A&B), demonstrating that the increased intensity within stratum lucidum is due to enriched pY816 immunoreactivity within mossy fiber axons (arrows point to pY816 enriched regions shown in Fig. 1 and Supplementary Fig. 1 to correspond anatomically to mossy fiber axons). Scale bar = 50 μm. E) Quantification of axonal pY816 immunoreactivity in $ZnT3^{+/+}$ (n=19) and $ZnT3^{-/-}$ (n=19) mice demonstrating an increase in the $ZnT3^{-/-}$ mouse compared to $ZnT3^{+/+}$ ($p<0.01$, Student's t-test). Quantification is presented as mean pY816 axonal immunoreactivity ± SEM. F) Percentages of synapsin-1 puncta within stratum lucidum found to be pY816+ in $ZnT3^{+/+}$ (n=19) and $ZnT3^{-/-}$ (n=19) animals. No significant differences in synaptic pY816 immunoreactivity was found in $ZnT3^{-/-}$ compared to $ZnT3^{+/+}$ mice ($p=0.77$, Student's t-test). A total of 5760 synapsin-1 puncta were analyzed in $ZnT3^{+/+}$ animals, and 5758 in $ZnT3^{-/-}$ mice. Quantification is presented as mean % ± SEM. All data were analyzed by Student's t-test; **$p<0.01$.

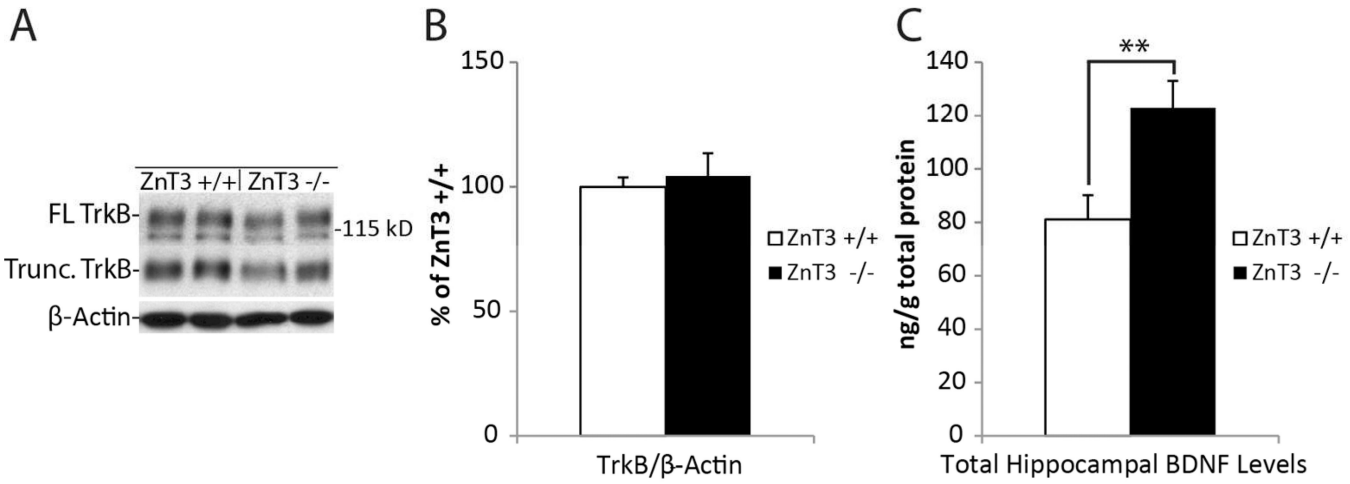

Figure 4. Total TrkB and BDNF levels in whole hippocampal homogenates comparing ZnT3$^{-/-}$ and ZnT3$^{+/+}$ animals

A) Representative Western blot demonstrating TrkB levels in ZnT3$^{+/+}$ and ZnT3$^{-/-}$ mice assayed in whole hippocampal lysates. FL TrkB = full length TrkB. Trunc. TrkB = truncated TrkB. B) Quantification of full-length TrkB levels demonstrates no significant difference between wild type (n=13) and knockout (n=11) animals. Data are represented as mean percent of average TrkB levels found in the ZnT3$^{+/+}$ animal ± SEM, and was normalized to β-actin as a loading control. C) Total BDNF levels in whole hippocampal lysates assayed by ELISA demonstrates an approximately 52% increase in the ZnT3$^{-/-}$ (n=10) compared to the ZnT3$^{+/+}$ (n=8) mouse. Data are represented as ng BDNF levels per gram of total protein ± SEM. All data were analyzed by Student's t-test; **p<0.01.

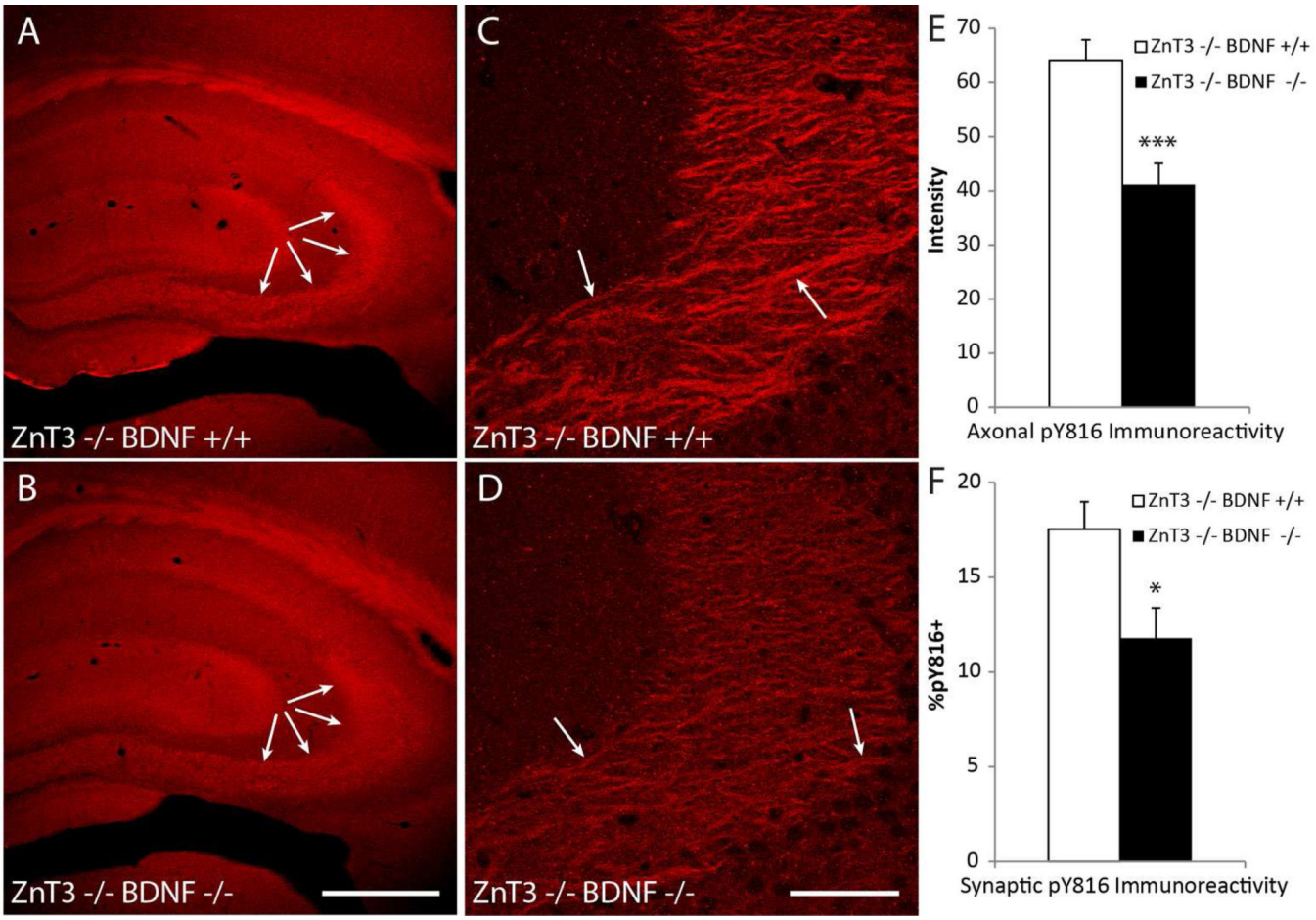

Figure 5. pY816 TrkB immunoreactivity in mossy fiber axons and synapses within stratum lucidum is decreased in ZnT3$^{-/-}$ BDNF$^{-/-}$ double knockouts compared to ZnT3$^{-/-}$ BDNF$^{+/+}$ single knockout mice

A&B) Representative low power micrographs of hippocampal sections from ZnT3$^{-/-}$ BDNF$^{+/+}$ (A) and ZnT3$^{-/-}$ BDNF$^{-/-}$ (B) mice stained with pY816, demonstrating that immunoreactivity within stratum lucidum of the ZnT3$^{-/-}$ BDNF$^{-/-}$ mouse (B, arrows) is diminished compared to its ZnT3$^{-/-}$ BDNF$^{+/+}$ littermate (A, arrows). Scale bar = 300 μm. C&D) Images of stratum lucidum taken at high power from hippocampal sections stained with pY816 from the same ZnT3$^{-/-}$ BDNF$^{+/+}$ (C) and ZnT3$^{-/-}$ BDNF$^{-/-}$ (D) mice as in (A&B) demonstrates that this observed reduction is due to decreased pY816 immunoreactivity within mossy fiber axons of the ZnT3$^{-/-}$ BDNF$^{-/-}$ double knockout (arrows point to pY816 enriched regions shown in Fig. 1 and Supplementary Fig. 1 to correspond anatomically to mossy fiber axons). Scale bar = 50 μm. E) Quantification of axonal pY816 immunoreactivity shows a significant decrease in immunoreactivity in ZnT3$^{-/-}$ BDNF$^{-/-}$ (n=11) compared to ZnT3$^{-/-}$ BDNF$^{+/+}$ (n=10) mice ($p<0.001$, Student's t-test). Quantification is presented as mean pY816 axonal immunoreactivity ± SEM. F) Quantification of percentages of synapsin-1 puncta within stratum lucidum found to contain pY816 immunoreactivity in ZnT3$^{-/-}$ BDNF$^{+/+}$ (n=8) and ZnT3$^{-/-}$ BDNF$^{-/-}$ (n=8) mice demonstrates a 32.6% reduction in synaptic pY816 immunoreactivity in the double knockout ($p<0.05$, Student's t-test). A total of 2400 synapsin-1 puncta were analyzed in

$ZnT3^{-/-}$ $BDNF^{+/+}$ animals and 2401 in $ZnT3^{-/-}$ $BDNF^{-/-}$ mice. Quantification is presented as mean % ± SEM. All data were analyzed by Student's t-test; ***$p<0.001$, *$p<0.05$.

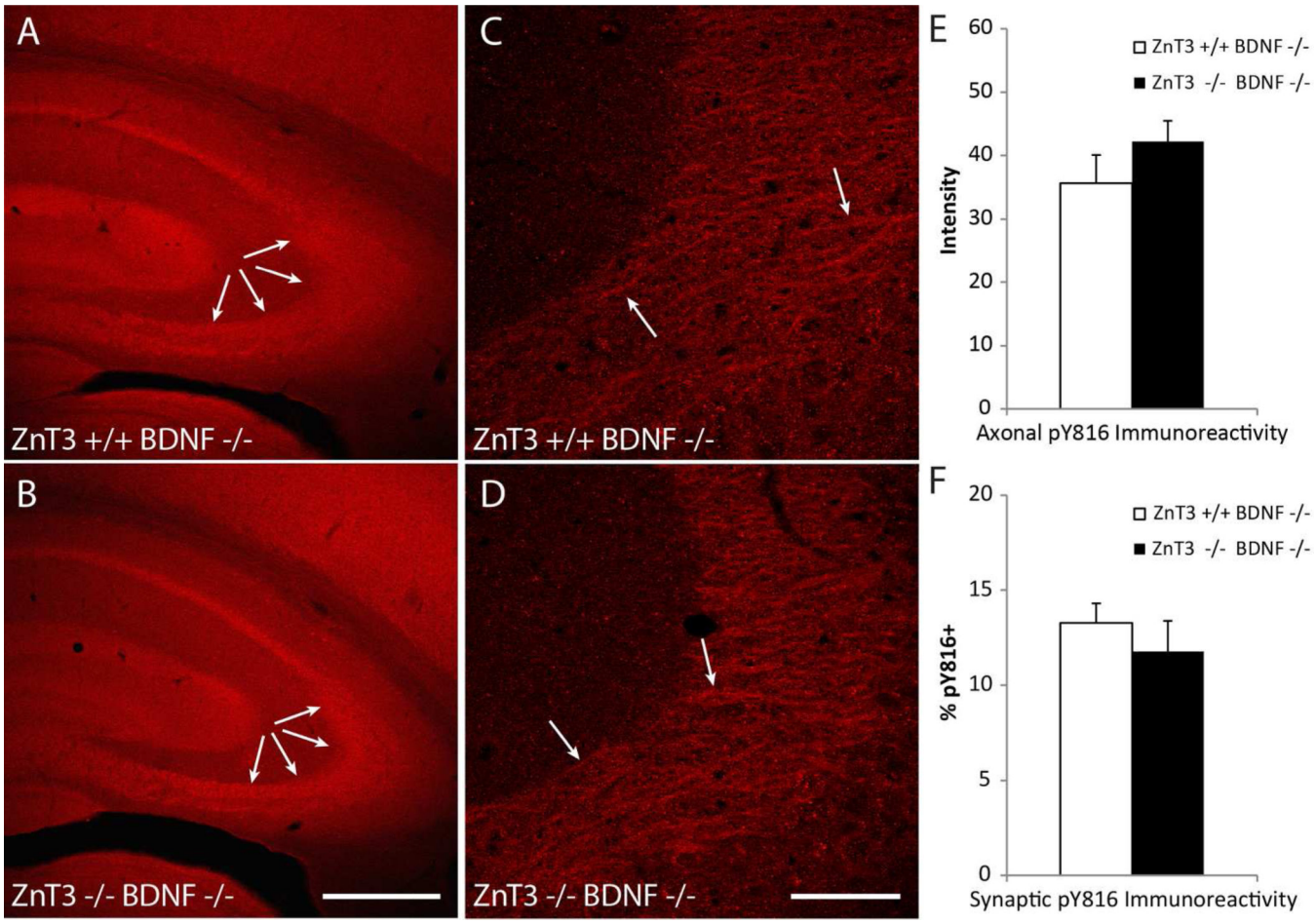

Figure 6. Axonal and synaptic pY816 TrkB immunoreactivity is not further reduced within stratum lucidum in ZnT3$^{-/-}$ BDNF$^{-/-}$ double knockouts compared to ZnT3$^{+/+}$ BDNF$^{-/-}$ single knockout mice

A&B) Representative low power images of hippocampi stained with pY816, taken from ZnT3$^{+/+}$ BDNF$^{-/-}$ (A) and ZnT3$^{-/-}$ BDNF$^{-/-}$ (B) mice. Immunoreactivity does not appear further changed in the double knockout (B, arrows) compared to the ZnT3$^{+/+}$ BDNF$^{-/-}$ animal (A, arrows). Scale bar = 300 μm. C&D) High power micrographs of stratum lucidum taken from pY816 stained sections from the same ZnT3$^{+/+}$ BDNF$^{-/-}$ (C) and ZnT3$^{-/-}$ BDNF$^{-/-}$ (D) animals as in (A&B), demonstrating that pY816 immunoreactivity within mossy fiber axons, already weak in the absence of BDNF, is not further changed in the absence of both ZnT3 and BDNF (arrows point to pY816 enriched regions shown in Fig. 1 and Supplementary Fig. 1 to correspond anatomically to mossy fiber axons). Scale bar = 50 μm. E) Quantification of axonal pY816 immunoreactivity in ZnT3$^{+/+}$ BDNF$^{-/-}$ (n=12) and ZnT3$^{-/-}$ BDNF$^{-/-}$ (n=12) mice reveals no change in the double compared to single knockout (p=0.25, Student's t-test). Quantification is presented as mean pY816 axonal immunoreactivity ± SEM. F) Percentages of synapsin-1 puncta within stratum lucidum found to be pY816+ in ZnT3$^{+/+}$ BDNF$^{-/-}$ (n=6) and ZnT3$^{-/-}$ BDNF$^{-/-}$ (n=8) mice. No significant difference in synaptic pY816 immunoreactivity was found between the two genotypes (p=0.48, Student's t- test). A total of 1800 synapsin-1 puncta were analyzed in

$ZnT3^{+/+}$ $BDNF^{-/-}$ mice, and 2401 in $ZnT3^{-/-}$ $BDNF^{-/-}$ animals. Quantification is presented as mean % ± SEM. All data were analyzed by Student's t-test.

Table 1

Primary antibodies.

Target	Immunogen	Source	Working Dilution
Phosphorylated tyrosine residue 816 of TrkB receptor (pY816)	LQNLAKASPVpYLDI, which corresponds to amino acids 806–819 of mouse TrkB receptor	McNamara Laboratory Rabbit Polyclonal	1:2000
Synapsin-1	Electrophoretically purified rat synapsin-1	Synaptic Systems (Cat# 106 001) Mouse Monoclonal RRID:AB_887805	1:500
Tau-1	Bovine microtubule associated proteins	Millipore (Cat# MAB3420) Mouse Monoclonal RRID:AB_94855	1:1000
TrkB	a.a. 54–67 of rat TrkB receptor	Chemicon (Cat# AB5372) Rabbit Polyclonal RRID:AB_91817	1:2000
Actin	C-terminal actin fragment attached to Multiple Antigen Peptide (MAP) backbone	Sigma (Cat# A2066) Rabbit Polyclonal RRID:AB_476693	1:5000

Table 2

Secondary antibodies.

Secondary Antibody	Source	Working Dilution
Alexa Fluor 555 Goat Anti-Rabbit IgG (H+L), highly cross-adsorbed	Invitrogen (Cat# A-21429) RRID:AB_141761	1:1000
Alexa Fluor 488 Goat Anti-Mouse IgG (H+L), highly cross-adsorbed	Invitrogen (Cat# A-11029) RRID:AB_138404	1:500
Alexa Fluor 633 Goat Anti-Mouse IgG (H+L), highly cross-adsorbed	Invitrogen (Cat# A-21052) RRID:AB_141459	1:500
Peroxidase Conjugated Goat Anti-Rabbit IgG	The Jackson Laboratory (Cat# 111-035-006) RRID:AB_2313586	1:5000